

MonoNeRF: Learning a Generalizable Dynamic Radiance Field from Monocular Videos

Fengrui Tian¹ Shaoyi Du¹ Yueqi Duan^{2*}

¹College of Artificial Intelligence, Xi'an Jiaotong University

²Department of Electronic Engineering, Tsinghua University

tianfr@stu.xjtu.edu.cn, dushaoyi@gmail.com, duanyueqi@tsinghua.edu.cn

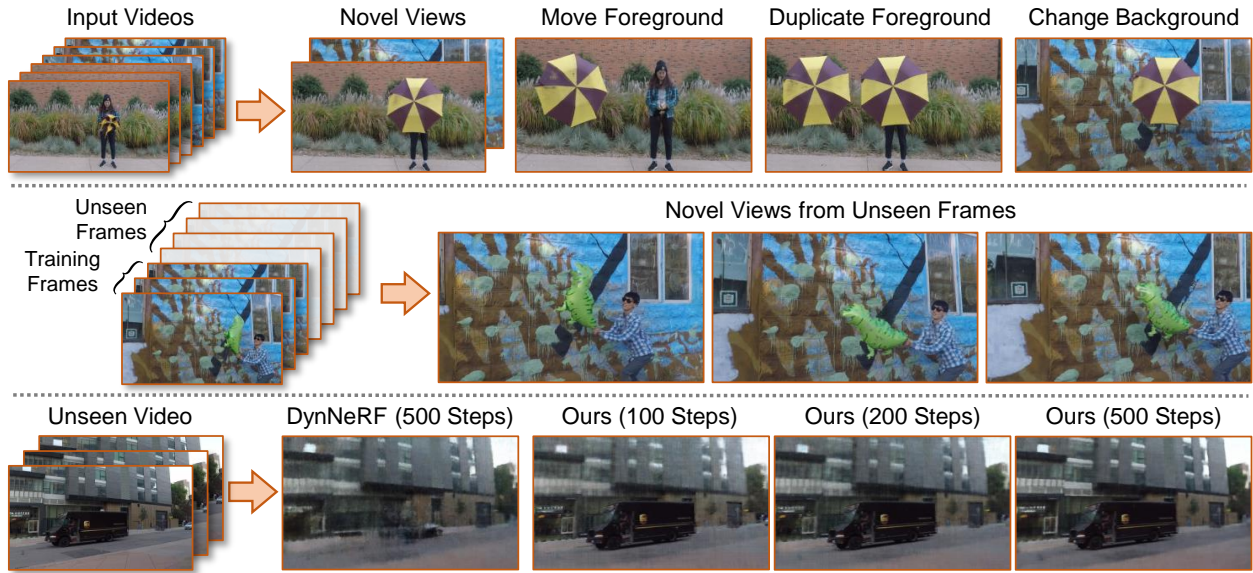


Figure 1. MonoNeRF learns a generalizable dynamic radiance field from multiple monocular videos. **Top:** scene editing including moving foreground, duplicating foreground and changing background. **Middle:** unseen frame synthesis by training on a few frames and testing on the following unseen frames. **Bottom:** novel scene adaptation by fine-tuning on an unseen video for hundreds of steps (about 10 minutes). The result of DynNeRF [13] is provided for comparison.

Abstract

In this paper, we target at the problem of learning a generalizable dynamic radiance field from monocular videos. Different from most existing NeRF methods that are based on multiple views, monocular videos only contain one view at each timestamp, thereby suffering from ambiguity along the view direction in estimating point features and scene flows. Previous studies such as DynNeRF disambiguate point features by positional encoding, which is not transferable and severely limits the generalization ability. As a result, these methods have to train one independent model for each scene and suffer from heavy computational costs when applying to increasing monocular videos in real-world applications. To address this, We propose MonoNeRF to

simultaneously learn point features and scene flows with point trajectory and feature correspondence constraints across frames. More specifically, we learn an implicit velocity field to estimate point trajectory from temporal features with Neural ODE, which is followed by a flow-based feature aggregation module to obtain spatial features along the point trajectory. We jointly optimize temporal and spatial features by training the network in an end-to-end manner. Experiments show that our MonoNeRF is able to learn from multiple scenes and support new applications such as scene editing, unseen frame synthesis, and fast novel scene adaptation.

*: Corresponding author. This work was done when Fengrui Tian was an intern at Shanghai Artificial Intelligence Laboratory.

1. Introduction

Novel view synthesis [6] is a highly challenging problem. It facilitates many important applications in movie production, sports event, and virtual reality. The long standing problem recently has witnessed impressive progress due to the neural rendering technology [9, 25, 27]. Neural Radiance Field (NeRF) [21, 26, 27, 42, 47, 48, 50] shows that photo-realistic scenes can be represented by an implicit neural network. Concretely, taken as a query the position and viewing direction of the posed image, the network outputs the color of each pixel by volume rendering method. Among these approaches, it is supposed that the scene is static and can be observed from multiple views at the same time. Such assumptions are violated by numerous videos uploaded to the Internet, which usually contain dynamic foregrounds, recorded by the monocular camera.

More recently, some studies aim to explore how to learn dynamic radiance field from monocular videos [10, 13, 20, 37, 45, 46]. Novel view synthesis from monocular videos is a challenging task. As foreground usually dynamically changes in a video, there is ambiguity in the view direction to estimate precise point features and dense object motions (*i.e.*, scene flow [40]) from single views. In other words, we can only extract the projected 2D intra-frame local features and inter-frame optical flows, but fail to obtain precise 3D estimations. Previous works address this challenge by representing points as 4D position features (coordinate and time), so that the learned positional encoding provides specific information for each 3D point in the space [10, 13, 20, 37, 45, 46]. Based on positional encoding, these methods make efforts on exploiting scene priors [12, 44, 45] or adding spatio-temporal regularization [10, 13, 20, 46] to learn a more accurate dynamic radiance field.

However, while positional encoding successfully disambiguates 3D points from monocular 2D projections, it severely overfits to the training video clip and is not transferable. Therefore, existing positional encoding based methods have to optimize one independent model for each dynamic scene. With the fast increase of monocular videos in reality, they suffer from heavy computational costs and lengthy training time to learn from multiple dynamic scenes. Also, the lack of generalization ability limits further applications of scene editing which requires interaction among different scenes. A natural question is raised: can we learn a generalizable dynamic radiance field from monocular videos?

In this paper, we provide a positive answer to this question. The key challenge of this task is to learn to extract generalizable point features in the 3D space from monocular videos. While independently using 2D local features and optical flows suffers from ambiguity along the ray direction, they provide complementary constraints to jointly learn 3D point features and scene flows. On the one hand, for the

sampled points on each ray, optical flow provides generalizable constraints that limit the relations of their point trajectories. On the other hand, for the flowing points on each estimated point trajectory, we consider that they should share the same point features. We estimate each point feature by aggregating their projected 2D local features, and design feature correspondence constraints to correct unreasonable trajectories.

To achieve this, we propose MonoNeRF to build a generalizable dynamic radiance field for multiple dynamic scenes. Our method concurrently predicts 3D point features and scene flows with point trajectory and feature correspondence constraints in monocular video frames. More specifically, we first propose to learn an implicit velocity field that encodes the speed from the temporal feature of each point. We supervise the velocity field with optical flow and integrate continuous point trajectories on the field with Neural ODE [5]. Then, we propose a flow-based feature aggregation module to sample spatial features of each point along the point trajectory. We incorporate the spatial and temporal features as the point feature to query the color and density for image rendering and jointly optimize point features and trajectories in an end-to-end manner. As shown in Figure 1, experiments demonstrate that our MonoNeRF is able to render novel views from multiple dynamic videos and support new applications such as scene editing, unseen frame synthesis, and fast novel scene adaption. Also, in the widely-used setting of novel view synthesis on training frames from single videos, our MonoNeRF still achieves better performance than existing methods despite that cross-scene generalization ability is not required in this setting.

2. Related Work

Novel view synthesis for static scenes. The long standing problem of novel view synthesis aims to construct new views of a scene from multiple posed images. Early work needed dense views captured from the scene [14, 18]. Recent studies have shown great progress by explicitly representing 3D scenes as neural representations [7, 9, 17, 24, 25, 27, 35, 47]. However, because these methods train a separate model for each scene, they need various training time for optimization. PixelNeRF [50] and MVSNeRF [4] proposed the feature based methods that directly inference new scenes from the encoded features. Additionally, many researchers studied the generalization and decomposition abilities of novel view synthesis model [1, 3, 15, 17, 28, 34]. Compared with these methods, our method studies the synthesis and generalization ability of dynamic scenes.

Space-time view synthesis from monocular videos. With the development of neural radiance field in static scene reconstruction, a series of studies started to address the dynamic scene reconstruction problem [10, 19, 20, 30, 31, 46]. Particularly in monocular videos, a key challenge is that

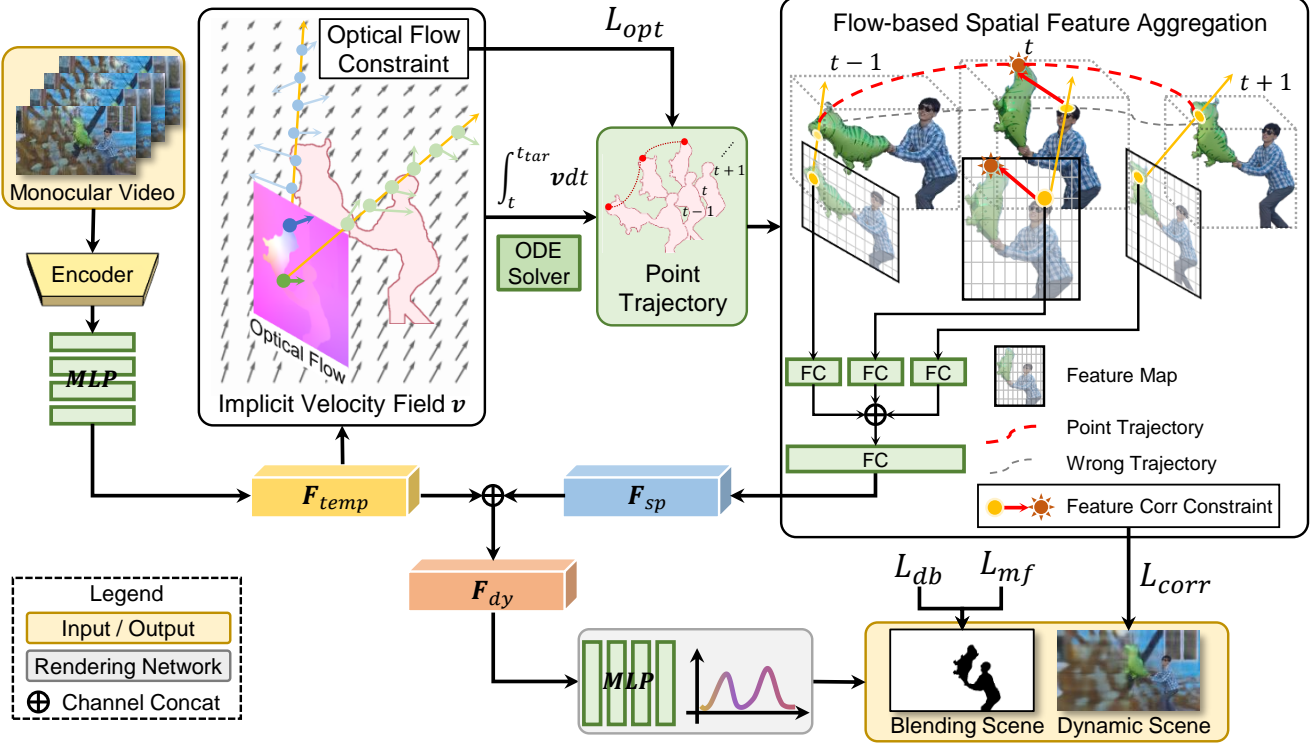


Figure 2. The overview of our generalizable dynamic field. We first exploit an implicit velocity field from the extracted temporal feature F_{temp} . Then, we calculate point trajectory on the velocity field, and exploit the spatial feature F_{sp} with the proposed flow-based spatial feature aggregation model. We incorporate spatial and temporal features as point feature F_{dy} for rendering dynamic scene and design L_{opt} and L_{corr} to jointly optimize point features and trajectories.

there exist multiple scene constructions that imply the same observed image sequences. Previous approaches addressed this challenge by representing point features as 3D coordinates with time and adding scene priors or spatio-temporal regularization to constrain motions. Scene priors such as shadow modeling [45], human shape prior [22, 44], and facial appearance [12] are object-specific and closer to special contents. Spatio-temporal regularization such as depth and flow regularization [10, 13, 20, 46] and object deformations [37] are more object-agnostic, but weaker in applying consistent restrictions to dynamic foreground. In this paper, we study the challenge by constraining point features.

Scene flow for reconstruction. Scene flow firstly proposed by [40] depicts the motion of each point in the dynamic scene. It with its 2D projection *i.e.*, optical flow contributes to many downstream applications such as video super-resolution [41], video tracking [38], video segmentation [39], and video recognition [2]. Several methods studied the scene flow estimation problem based on point cloud sequences [23, 29]. However, estimating scene flow from the observed video is an ill-posed problem. In dynamic scene reconstruction, previous works [13, 20] established discrete scene flow for pixel consistency in obser-

vation time. In this way, the flow consistency between two adjacent frames can only be constrained, leading to ambiguity in non-observed time. Du *et al.* [10] proposed a method called NeRFlow that builds the continuous flow field in dynamic scene. Our method presents a generalizable flow field that implicitly models the continuous point trajectory.

3. Approach

In this section, we introduce the proposed model that we term as MonoNeRF. We first present the overview of our model, and then detail the approach of each part. Lastly, we introduce several strategies for optimizing the model.

3.1. MonoNeRF

MonoNeRF aims to model point features in the dynamic scene for rendering free-point videos. Our method takes as input multiple monocular videos with binary masks of the foreground objects and builds the generalizable static and dynamic fields for backgrounds and foregrounds separately. The foreground mask can be received automatically by motion segmentation methods. For generalizable dynamic field, we first learn an implicit velocity field with temporal features extracted by a 3D CNN encoder. Then,

we calculate the point trajectory on the field and propose a flow-based feature aggregation model to sample spatial features along the point trajectory. We aggregate the spatial and temporal features as point features to render foreground scenes with a neural radiance field. For static background that may be occluded by the moving objects, we propose to sample geometric consistent point features. Finally we combine the generalizable static and dynamic fields and provide the consistency restrictions to train the entire model. In the following sections, we will use boldface type for vectors or vector functions and regular type for scalars or scalar functions.

3.2. Generalizable Dynamic Field

In this section, we introduce our generalizable dynamic field that renders novel views of dynamic foreground.

Implicit velocity field. We suppose points are moving in the scene and denote a spatio-temporal point $\mathbf{p} = [\mathbf{x}_p, t_i]$ as the 3D point position \mathbf{x} at time t_i . We define Φ as the point trajectory and $\Phi(\mathbf{p}, t)$ is the position of point \mathbf{p} at timestamp t . We further define the velocity field \mathbf{v} which includes the 3D velocity of each point. The relationship between point velocity and trajectory is specified by the following equation,

$$\frac{\partial \Phi(\mathbf{p}, t)}{\partial t} = \mathbf{v}(\Phi(\mathbf{p}, t), t), \quad \text{s.t. } \Phi(\mathbf{p}, t_i) = \mathbf{x}_p. \quad (1)$$

As Figure 2 shows, we exploit a multiple layer perceptron (MLP) that outputs the temporal feature $\mathbf{F}_{temp}(\mathbf{p})$ of each point. Then, we build the velocity field based on the temporal feature. We supervise \mathbf{v} with the optical flow. Concretely, given a ray $\mathbf{r} = \mathbf{o} + u\mathbf{d}$ starting from camera center \mathbf{o} through a pixel on the image at time t , the integrated velocity along the ray is calculated by the following equation,

$$\hat{\mathbf{f}}(\mathbf{r}) = \int_{u_n}^{u_f} T_{dy}(u) \sigma_{dy}(u) \mathbf{v}(\mathbf{r}(u), t) du, \quad (2)$$

where $\sigma_{dy}(u)$ is the estimated volume rendering density and $T_{dy}(u) = \exp(-\int_{u_n}^u \sigma_{dy}(\mathbf{r}(s)) ds)$ is the accumulated transparency. u_n, u_f are the bounds of the volume rendering depth range. We simplify $\sigma(u) = \sigma(\mathbf{r}(u))$ here and in the following sections. We project $\hat{\mathbf{f}}$ to the 2D image plane with the projection matrix as the estimated optical flow and supervise it by the ground truth flow,

$$L_{opt} = \sum_{\mathbf{r}} \left(\hat{\mathbf{f}}(\mathbf{r}) - \mathbf{f}(\mathbf{r}) \right), \quad (3)$$

where $\mathbf{f}(\mathbf{r})$ denotes the optical flow from ground truth. However in practice, \mathbf{f} can only be approximated between image pairs [36] to generate the backward flow \mathbf{f}_{bw} and forward flow \mathbf{f}_{fw} . We hence extract point trajectory variations between image pairs as the pseudo flows. Given

the video frame sequence with the observed timestamps $\{t_i, i = 0, \dots, T-1\}$, for each point on the ray (i.e., $\mathbf{p}(u) = [\mathbf{r}(u), t_i]$) the trajectory variations $\Delta \Phi_{bw}$ back to t_{i-1} and $\Delta \Phi_{fw}$ forward to t_{i+1} are obtained as follows,

$$\Delta \Phi_{\{bw, fw\}}(\mathbf{p}(u)) = \int_{t_i}^{t_{\{i-1, i+1\}}} \mathbf{v}(\Phi(\mathbf{p}(u), t), t) dt. \quad (4)$$

The equation can be solved by using Neural ODE [5] and the pseudo optical flow is obtained by

$$\hat{\mathbf{f}}_{\{bw, fw\}}(\mathbf{r}) = \int_{u_n}^{u_f} T_{dy}(u) \sigma_{dy}(u) \Delta \Phi_{\{bw, fw\}}(\mathbf{p}(u)) du. \quad (5)$$

We represent $\hat{\mathbf{f}}_{\{bw, fw\}}$ as $\hat{\mathbf{f}}$ to conduct the flow constraint.

Flow-based spatial feature aggregation. The point trajectory at t_{tar} can be calculated as follows,

$$\Phi(\mathbf{p}, t_{tar}) = \int_{t_i}^{t_{tar}} \mathbf{v}(\Phi(\mathbf{p}, t), t) dt + \mathbf{x}_p. \quad (6)$$

We extract the frame-wise image features by the encoder. For each point \mathbf{p} , we calculate its corresponding position at the observed timestamp t_j as $\Phi(\mathbf{p}, t_j)$ and project the point to the 2D image with the projection matrix. As shown in Figure 2, we sample the projected features at the corresponding positions on the feature maps, and fuse the pixel features with fully connected layers. Finally we term the fused features as the spatial feature $\mathbf{F}_{sp}(\mathbf{p})$ and incorporate the spatial and temporal features as the point feature $\mathbf{F}_{dy}(\mathbf{p})$ in the generalizable dynamic field,

$$\mathbf{F}_{dy}(\mathbf{p}) = \text{concat}\{\mathbf{F}_{temp}(\mathbf{p}), \mathbf{F}_{sp}(\mathbf{p})\}. \quad (7)$$

We render the dynamic scene with the point feature \mathbf{F}_{dy} .

Dynamic foreground rendering. To render the dynamic foreground, we represent the dynamic scene as a radiance field that takes as input the point with its feature $\mathbf{F}_{dy}(\mathbf{p})$ to predict the volume density σ_{dy} , color \mathbf{c}_{dy} and blending weight b by using an MLP $\mathbf{W}_{dy} : (\mathbf{p}, \mathbf{F}_{dy}(\mathbf{p})) \rightarrow (\mathbf{c}_{dy}, \sigma_{dy}, b)$. We follow [13] that utilizes blending weight to judge whether the point belongs to static background or dynamic foreground. We then use volume rendering technology to approximate the color of each pixel,

$$\hat{\mathbf{C}}_{dy}(\mathbf{r}) = \int_{u_n}^{u_f} T_{dy}(u) \sigma_{dy}(u) \mathbf{c}_{dy}(u) du. \quad (8)$$

We simplify $\mathbf{c}(u) = \mathbf{c}(\mathbf{r}(u), \mathbf{d})$ here and in the following sections. The reconstruction loss of the generalizable dynamic field is the difference between the predicted color $\hat{\mathbf{C}}_{dy}$ and the ground truth color \mathbf{C}_{dy} ,

$$L_{curr} = \sum_{\mathbf{r}} \|\hat{\mathbf{C}}_{dy}(\mathbf{r}) - \mathbf{C}_{dy}(\mathbf{r})\|_2. \quad (9)$$

L_{curr} supervises the color encoded by the point feature at current time. We suppose a point moving along the trajectory renders consistent color and density by the corresponding point feature. Concretely, for each ray \mathbf{r} at time t_i , we warp the ray from neighboring observed timestamps $t_{\{i-1, i+1\}}$ as $\mathbf{r}_{\{bw, fw\}}$ by using the trajectory variations (4),

$$\mathbf{r}_{\{bw, fw\}}(u) = \mathbf{r}(u) + \Delta\Phi_{\{bw, fw\}}(\mathbf{p}(u)). \quad (10)$$

We exploit the point feature at each position $\mathbf{r}_{\{bw, fw\}}(u)$ and time $t_{\{i-1, i+1\}}$. Then we query the color and density from the corresponding point features to render the pixel color by using (8) and supervise the color with the ground truth,

$$L_{\{bw, fw\}} = \sum_{\mathbf{r}} \|\hat{\mathbf{C}}_{dy}(\mathbf{r}_{\{bw, fw\}}) - \mathbf{C}_{dy}(\mathbf{r})\|_2, \quad (11)$$

where $\hat{\mathbf{C}}_{dy}(\mathbf{r}_{\{bw, fw\}})$ is the predicted pixel color from the point feature at $t_{\{i-1, i+1\}}$. Hence the feature corresponding constraint L_{corr} is defined as:

$$L_{corr} = L_{bw} + L_{fw} + L_{curr}. \quad (12)$$

L_{corr} supervises the predicted image color encoded by the corresponding point features. Hence it also indirectly rectifies the wrong point trajectories.

3.3. Generalizable Static Field

Different from the dynamic foreground, we suppose the background is static in the video, where the point feature ought to hold geometric consistency among all video frames. For some parts of the background scene that are occluded by the changing foreground in the current view, their features implying the foreground cannot infer the correct background information. However, the occlusion parts could be seen in other views with correct background features. To achieve this, given the static point position \mathbf{x} , we sample the background point feature $\mathbf{F}_{st}(\mathbf{x})$ from other frames extracted by a 2D CNN encoder,

$$\mathbf{F}_{st}(\mathbf{x}) = \mathbf{F}_{other}(\mathbf{x}), \quad (13)$$

where \mathbf{F}_{other} denotes the feature sampling from the feature maps in other frames. We select the frames randomly in this study. Then, we represent the static scene as a radiance field based on the feature. Concretely, taking as input the point feature with its position \mathbf{x} and viewing direction \mathbf{d} , \mathbf{F}_{st} infers the color \mathbf{c} and density σ with the MLP $\mathbf{W}_{st} : (\mathbf{x}, \mathbf{d}, \mathbf{F}_{st}(\mathbf{x})) \rightarrow (\mathbf{c}_{st}, \sigma_{st})$. The expected background color $\hat{\mathbf{C}}_{st}$ of is given by

$$\hat{\mathbf{C}}_{st}(\mathbf{r}) = \int_{u_n}^{u_f} T_{st}(u) \sigma_{st}(u) \mathbf{c}_{st}(u) du, \quad (14)$$

where $T_{st}(t) = \exp(-\int_{u_n}^t \sigma_{st}(\mathbf{r}(s)) ds)$. Reconstruction loss is the color difference between the predicted color and the ground truth,

$$L_{st} = \sum_{\mathbf{r}} \|\hat{\mathbf{C}}_{st}(\mathbf{r}) - \mathbf{C}_{st}(\mathbf{r})\|_2, \quad (15)$$

where \mathbf{C}_{st} is the ground truth color.

3.4. Optimization

The final dynamic scene color combines the generalizable dynamic and static fields,

$$\hat{\mathbf{C}}_{full}(\mathbf{r}) = \int_{u_n}^{u_f} T_{full}(u) \sigma_{full}(u) \mathbf{c}_{full}(u) du, \quad (16)$$

where

$$\sigma_{full}(u) \mathbf{c}_{full}(u) = (1 - b) \sigma_{st}(u) \mathbf{c}_{st}(u) + b \sigma_{dy}(u) \mathbf{c}_{dy}(u), \quad (17)$$

and applies the reconstruction loss,

$$L_{full} = \sum_{\mathbf{r}} \|\hat{\mathbf{C}}_{full}(\mathbf{r}) - \mathbf{C}_{full}(\mathbf{r})\|_2. \quad (18)$$

In the following, we design several strategies to optimize our model in both inference time and image rendering quality.

Point trajectory discretization. While point trajectory can be numerically estimated by the continuous integral (6) with Neural ODE solvers [5], it needs plenty of inference time for querying each point in space and time. To accelerate the inference process during rendering images, we exploit a stratified sampling approach where we partition $[t_i, t_{tar}]$ into N evenly-spaced bins and suppose the point velocity in each bin is a constant. The point trajectory can be estimated by the following equation,

$$\Phi(\mathbf{p}, t_{tar}) = \sum_{n=1}^N \mathbf{v}(\Phi(\mathbf{p}, t + \Delta t), t + \Delta t) \Delta t + \mathbf{x}_p, \quad (19)$$

where $\Delta t = \frac{n}{N}(t_{tar} - t_i)$.

Depth-blending restriction. We suppose all the foreground point positions are around the depth map margin of each view. Given the pixel ground truth depth u_d on the image with the rays $\mathbf{r}(u)$ through that pixel, we suppose the points on the ray out of $(u_d - \epsilon, u_d + \epsilon)$ are the static points, where the blending weights should be penalized,

$$L_{db} = \sum_{u \in (u_n, u_d - \epsilon) \cup (u_d + \epsilon, u_f)} \|b(\mathbf{r}(u))\|_2, \quad (20)$$

where $b(\mathbf{r}(u))$ is the blending weight at the position $\mathbf{r}(u)$. ϵ controls the surface thickness of the dynamic foreground.

Table 1. Novel view synthesis on training frames from single videos. While this setting does not require cross-scene generalization ability, our MonoNeRF still achieves better performance.

PSNR \uparrow / LPIPS \downarrow	Jumping	Skating	Truck	Umbrella	Balloon1	Balloon2	Playground	Average
NeRF [27]	20.58 / 0.305	23.05 / 0.316	22.61 / 0.225	21.08 / 0.441	19.07 / 0.214	24.08 / 0.098	20.86 / 0.164	21.62 / 0.252
NeRF [27] + time	16.72 / 0.489	19.23 / 0.542	17.17 / 0.403	17.17 / 0.752	17.33 / 0.304	19.67 / 0.236	13.80 / 0.444	17.30 / 0.453
Yoon <i>et al.</i> [49]	20.16 / 0.148	21.75 / 0.135	23.93 / 0.109	20.35 / 0.179	18.76 / 0.178	19.89 / 0.138	15.09 / 0.183	19.99 / 0.153
Tretschk <i>et al.</i> [37]	19.38 / 0.295	23.29 / 0.234	19.02 / 0.453	19.26 / 0.427	16.98 / 0.353	22.23 / 0.212	14.24 / 0.336	19.20 / 0.330
Li <i>et al.</i> [20]	24.12 / 0.156	28.91 / 0.135	25.94 / 0.171	22.58 / 0.302	21.40 / 0.225	24.09 / 0.228	20.91 / 0.220	23.99 / 0.205
DynNeRF [13]	24.23 / 0.144	28.90 / 0.124	25.78 / 0.134	23.15 / 0.146	21.47 / 0.125	25.97 / 0.059	23.65 / 0.093	24.74 / 0.118
MonoNeRF	24.26 / 0.091	32.06 / 0.044	27.56 / 0.115	23.62 / 0.180	21.89 / 0.129	27.36 / 0.052	22.61 / 0.130	25.62 / 0.106

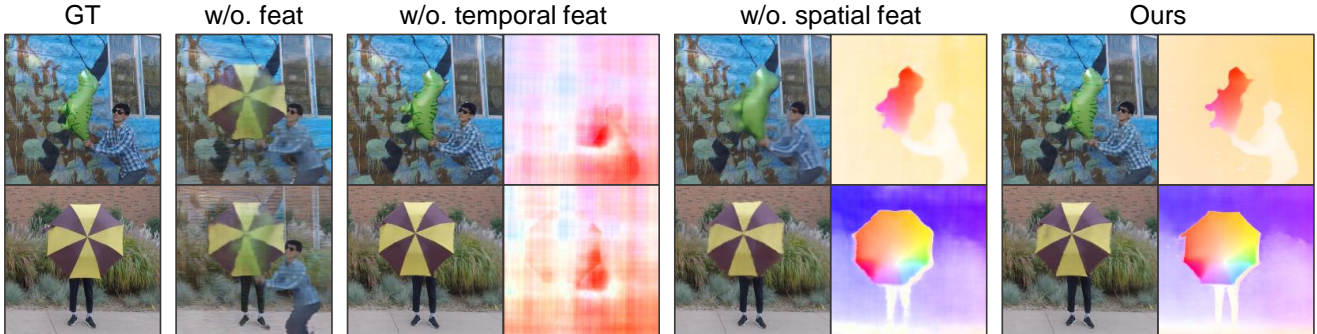


Figure 3. Qualitative results of our model on Balloon2 and Umbrella scenes. Our method renders more accurate novel views and predict plausible scene flows by incorporating temporal and spatial features.

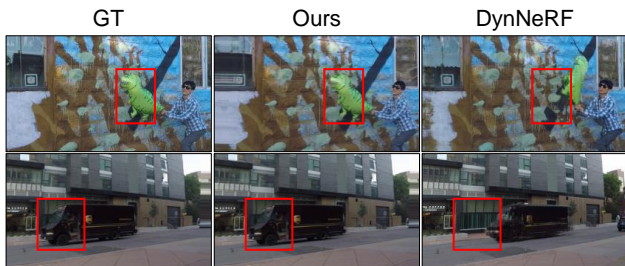


Figure 4. Novel view synthesis on unseen frames. Compared to the ground truths, our model could transfer to new motions, whereas DynNeRF [13] only interpolates in the training frames.

Mask flow loss. We believe that a point moving along the trajectory has consistent blending weight, which is constrained by the following equation,

$$L_{mf} = \sum_{i,j \in [0, T-1]} \|b(\Phi(\mathbf{p}, t_i)) - b(\Phi(\mathbf{p}, t_j))\|_2, \quad (21)$$

where we denote $b(\Phi(\mathbf{p}, t))$ as the blending weight at $\Phi(\mathbf{p}, t)$.

Other regularization. We follow the common practices [10, 13, 20] to use depth-supervised loss and sparsity regularization to train the model, and motion regularization and smoothness [13, 20] to supervise the trajectory.

Table 2. Quantitative results of novel view synthesis on unseen frames. We used the first four frames for training and tested the novel view synthesis performance on the rest eight frames.

Balloon2 / Truck	PSNR \uparrow	SSIM \uparrow	LPIPS \downarrow
NeRF [27]	20.33 / 20.26	0.662 / 0.669	0.224 / 0.256
NeRF [27] + time	20.22 / 20.26	0.661 / 0.639	0.218 / 0.256
DynNeRF [13]	19.99 / 20.33	0.641 / 0.621	0.291 / 0.273
Ours	21.30 / 23.74	0.669 / 0.702	0.204 / 0.174

4. Experiments

In this section, we conducted experiments on the Dynamic Scene dataset [49]. We first tested the performance of synthesizing novel views from single videos on both training frames and unseen frames, and then we tested the generalization ability from multiple videos. Finally we carried out ablation studies on our model.

4.1. Experimental Setup

Dataset. We used the Dynamic Scene dataset [49] to evaluate the proposed method. It contains 9 video sequences that are captured with 12 cameras by using a camera rig. All the cameras capture images at 12 different timestamps $\{t_i, i = 0, 1, \dots, 11\}$. The training data of each input video contains twelve frames $\{I_i, i = 0, 1, \dots, 11\}$ sampled from the i^{th} camera at time t_i . It is noticed that each frame of the video is derived from different cameras

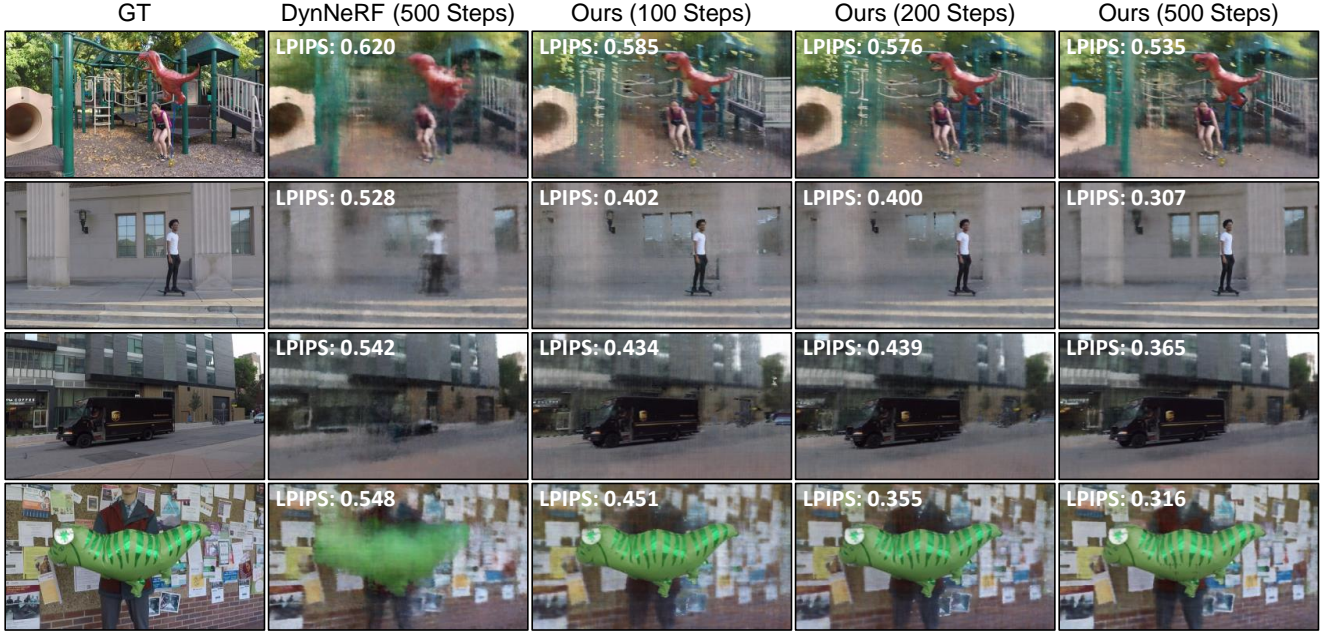


Figure 5. Fast novel scene adaption. We used the pretrained model on Balloon2 scene to fine-tune the novel views of unseen dynamic scenes. We employed LPIPS [51] (the lower is better) to evaluate the image similarity, which provides more correlation with human judgment than other indexes.

to simulate the camera motion. Each input frame includes a still background and a time-varying foreground. We followed [20, 27] and used COLMAP [32, 33] to approximate the camera poses. It is assumed intrinsic parameters of all the cameras are the same. DynamicFace sequences were excluded because COLMAP fails to estimate camera poses. All video frames were resized to 480×270 resolution.

Implementation details. For generalizable dynamic field, we utilized SlowFast50 [11] as our backbone, which was pretrained on Kinetics400 [2] dataset. We removed the final fully connected layer in the backbone and incorporated the first, second, and third feature layers for querying the spatial point features. The spatial feature of the point at time t_i is sampled in the feature maps at time $\{t_{i-1}, t_i, t_{i+1}\}$. We generated optical flows from image pairs by using [36]. For generalizable static field, we used ResNet18 [16] as the backbone encoder. The backbone was pretrained on ImageNet [8]. We extracted a feature pyramid from the input image to sample the static point feature. We followed [50] and used ResNet-based fully connected layer as our rendering network.

4.2. Novel View Synthesis from Single Video

In this section, we trained the models from single monocular videos, where existing methods are applicable to this setting. Specifically, we first tested the performance of our model on training frames with other state-of-the-art methods, which is the widely-used setting to evaluate

Table 3. Ablation studies on temporal and spatial features. We conducted the experiments on the Balloon2 and Umbrella scenes.

PSNR \uparrow / LPIPS \downarrow	Umbrella	Balloon2	Average
w/o. feat	19.18 / 0.578	20.72 / 0.370	19.95 / 0.474
w/o. temp feat	22.75 / 0.175	24.85 / 0.098	23.80 / 0.137
w/o. sp feat	22.81 / 0.181	25.09 / 0.143	23.95 / 0.162
Ours	23.44 / 0.169	25.44 / 0.093	24.44 / 0.131

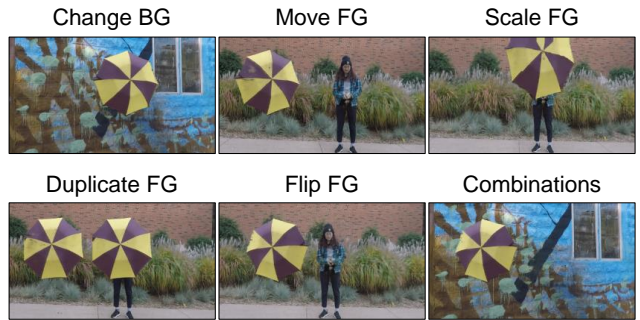


Figure 6. Our model supports many scene editing applications such as background changing, foreground moving, scaling, duplicating, and flipping, and arbitrary combinations.

video-based NeRFs. Then, we tested the generation ability on unseen frames in the video, where other existing methods are not able to transfer well to the unseen motions.

Novel View Synthesis on Training Frames. To evalu-

Table 4. Comparisons of solving the continuous trajectory by using ODE solver [5] and our discretization method.

Method	PSNR \uparrow	SSIM \uparrow	LPIPS \downarrow
$N = 1$	22.90	0.7524	0.134
$N = 2$	22.97	0.7551	0.134
$N = 4$	23.00	0.7550	0.136
ODE solver [5]	23.75	0.7716	0.136

ate the synthesized novel views, we tested the performance by fixing the view to the first camera and changing time following [13]. We reported the PSNR and LPIPS [51] on seven scenes in Table 1. We evaluated the performance of Li *et al.* [20], Tretschk *et al.* [37], and Chen *et al.* [13] from the official implementations. Even without the need of generalization ability, our method achieves better results.

Novel View Synthesis on Unseen Frames. To test the generation ability, we split the input video frames into two groups: the front four frames were used for training and the rest of eight frames were utilized to test the generation ability in unseen motions. Figure 4 shows our model could directly render new motions in the unseen frames from the point features, while DynNeRF [13] only interpolates novel views in the training frames. Table 2 shows the quantitative results on unseen frames. We reported PSNR, SSIM [43] and LPIPS scores. It shows that our model outperforms other methods by a large margin.

4.3. Novel View Synthesis from Multiple Videos

In the section, we tested the novel view synthesis performance on multiple dynamic scenes. It is worth noting that as existing methods can only learn from single monocular videos, they are not applicable to the settings that need to train on multiple videos. Then, we evaluated the novel scene adaption ability on several novel monocular videos. Lastly, we conducted a series of scene editing experiments.

Novel View Synthesis on Training Videos. We selected Balloon2 and Umbrella scenes to train our model. As Figure 3 shows, we trained our model in four situations: without point features F_{dy} and F_{st} , without temporal features F_{temp} , without spatial features F_{sp} and with point features. It can be seen that our point feature contributes to building a generalizable radiance field from multiple videos. Moreover, our model could generate generalizable scene flows with the temporal feature, and render more accurate image details with the spatial feature. Table 3 quantitatively demonstrates the effectiveness of our temporal and spatial features.

Novel View Synthesis on Unseen Videos. We tested the generalization ability of our model by pretraining on the Balloon2 scene and finetuning the pretrained model on other scenes. Figure 5 presents the results of four unseen videos: Playground, Skating, Truck and Balloon1. We also

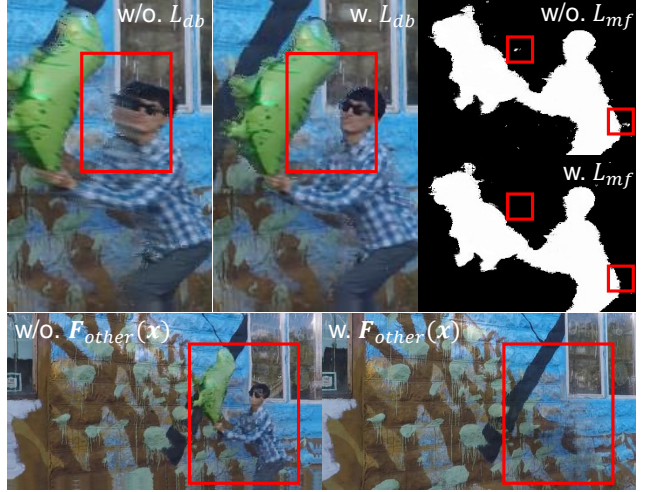


Figure 7. Ablation studies on L_{db} , L_{mf} , and F_{other} .

pretrained DynNeRF [13] on Balloon2 scene for an apple-to-apple comparison. We reported the LPIPS score of each image, which correlates more with human perception judgment than other indexes. It can be seen that our model could transfer to new scenes with correct dynamic motions, while DynNeRF only learns to render the new scenes from scratch. By further training with 500 steps, our model achieves better image rendering quality and higher LPIPS score, which takes about 10 minutes.

Scene Editing. As Figure 6 shows, our model further supports many scene editing applications by directly processing the point features without extra training. Changing background was implemented by exchanging the static scene features between two scenes. Moving, scaling, duplicating and flipping foreground were directly applied by operating video features in generative dynamic radiance field. The above applications could be combined arbitrarily.

4.4. Ablation Study

We conducted a series of experiments to examine the proposed L_{db} , L_{mf} , and static point features. In Figure 7, It can be seen that L_{db} deblurs the margin of the synthesized foreground in novel views, L_{mf} keeps the blending consistency in different views for delineating the foreground more accurately, and using F_{rand} could successfully render static scene without dynamic foreground. We also tested the effectiveness of our point trajectory discretization method on Balloon1 and Balloon2 scenes. In Table 4, our discretization method reaches comparable results with ODE solvers [5], and achieves higher performance on PSNR, SSIM, and LPIPS indexes with the increase of N .

5. Conclusion

In this paper, we study the generalization ability of novel view synthesis from monocular videos. The challenge is the ambiguity of 3D point features and scene flows in the viewing directions. We find that 2D video frame features and optical flows are a pair of complementary constraints for learning 3D point features and scene flows. To achieve this, we propose a generalizable dynamic radiance field called MonoNeRF. We first extract an implicit velocity field from the extracted temporal feature. Then we calculate point trajectories on the field and sample the spatial features along the trajectories. We fuse the temporal and spatial features as the final point feature to render dynamic scenes from novel views. Experiments show that our model could learn a generalizable radiance field for single or multiple dynamic scenes, and support many scene editing applications.

References

- [1] Shengqu Cai, Anton Obukhov, Dengxin Dai, and Luc Van Gool. Pix2NeRF: Unsupervised conditional π -GAN for single image to neural radiance fields translation. In *CVPR*, pages 3971–3980, 2022. 2
- [2] Joao Carreira and Andrew Zisserman. Quo vadis, action recognition? a new model and the kinetics dataset. In *CVPR*, pages 6299–6308, 2017. 3, 7
- [3] Eric Chan, Marco Monteiro, Petr Kellnhofer, Jiajun Wu, and Gordon Wetzstein. pi-GAN: Periodic implicit generative adversarial networks for 3D-aware image synthesis. In *CVPR*, 2021. 2
- [4] Anpei Chen, Zexiang Xu, Fuqiang Zhao, Xiaoshuai Zhang, Fanbo Xiang, Jingyi Yu, and Hao Su. MVSNeRF: Fast generalizable radiance field reconstruction from multi-view stereo. In *ICCV*, pages 14124–14133, 2021. 2
- [5] Ricky T. Q. Chen, Yulia Rubanova, Jesse Bettencourt, and David K Duvenaud. Neural ordinary differential equations. In S. Bengio, H. Wallach, H. Larochelle, K. Grauman, N. Cesa-Bianchi, and R. Garnett, editors, *NeurIPS*, volume 31, 2018. 2, 4, 5, 8
- [6] Shenchang Eric Chen and Lance Williams. View interpolation for image synthesis. In *Proceedings of the 20th annual conference on Computer graphics and interactive techniques*, pages 279–288, 1993. 2
- [7] Xingyu Chen, Qi Zhang, Xiaoyu Li, Yue Chen, Ying Feng, Xuan Wang, and Jue Wang. Hallucinated neural radiance fields in the wild. In *CVPR*, pages 12943–12952, 2022. 2
- [8] Jia Deng, Wei Dong, Richard Socher, Li-Jia Li, Kai Li, and Li Fei-Fei. ImageNet: A large-scale hierarchical image database. In *CVPR*, pages 248–255, 2009. 7
- [9] Kangle Deng, Andrew Liu, Jun-Yan Zhu, and Deva Ramanan. Depth-supervised NeRF: Fewer views and faster training for free. In *CVPR*, June 2022. 2
- [10] Yilun Du, Yinan Zhang, Hong-Xing Yu, Joshua B. Tenenbaum, and Jiajun Wu. Neural radiance flow for 4d view synthesis and video processing. In *ICCV*, 2021. 2, 3, 6
- [11] Christoph Feichtenhofer, Haoqi Fan, Jitendra Malik, and Kaiming He. SlowFast networks for video recognition. In *ICCV*, pages 6201–6210, 2019. 7
- [12] Guy Gafni, Justus Thies, Michael Zollhöfer, and Matthias Nießner. Dynamic neural radiance fields for monocular 4d facial avatar reconstruction. In *CVPR*, pages 8649–8658, June 2021. 2, 3
- [13] Chen Gao, Ayush Saraf, Johannes Kopf, and Jia-Bin Huang. Dynamic view synthesis from dynamic monocular video. In *ICCV*, 2021. 1, 2, 3, 4, 6, 8
- [14] Steven J Gortler, Radek Grzeszczuk, Richard Szeliski, and Michael F Cohen. The lumigraph. In *ACM SIGGRAPH*, pages 43–54, 1996. 2
- [15] Jiatao Gu, Lingjie Liu, Peng Wang, and Christian Theobalt. StyleNeRF: A style-based 3D aware generator for high-resolution image synthesis. In *ICLR*, 2022. 2
- [16] Kaiming He, X. Zhang, Shaoqing Ren, and Jian Sun. Deep residual learning for image recognition. *CVPR*, pages 770–778, 2016. 7
- [17] Wonbong Jang and Lourdes Agapito. CodeNeRF: Disentangled neural radiance fields for object categories. In *ICCV*, pages 12949–12958, October 2021. 2
- [18] Marc Levoy and Pat Hanrahan. Light field rendering. In *ACM SIGGRAPH*, 1996. 2
- [19] Tianye Li, Mira Slavcheva, Michael Zollhöfer, Simon Green, Christoph Lassner, Changil Kim, Tanner Schmidt, Steven Lovegrove, Michael Goesele, Richard Newcombe, and Zhaoyang Lv. Neural 3D video synthesis from multi-view video. In *CVPR*, pages 5521–5531, June 2022. 2
- [20] Zhengqi Li, Simon Niklaus, Noah Snavely, and Oliver Wang. Neural scene flow fields for space-time view synthesis of dynamic scenes. In *CVPR*, 2021. 2, 3, 6, 7, 8
- [21] Lingjie Liu, Jiatao Gu, Kyaw Zaw Lin, Tat-Seng Chua, and Christian Theobalt. Neural sparse voxel fields. In *NeurIPS*, volume 33, 2020. 2
- [22] Lingjie Liu, Marc Habermann, Viktor Rudnev, Kripasindhu Sarkar, Jiatao Gu, and Christian Theobalt. Neural actor: Neural free-view synthesis of human actors with pose control. *ACM Trans. Graph.(ACM SIGGRAPH Asia)*, 2021. 3
- [23] Xingyu Liu, Charles R Qi, and Leonidas J Guibas. FlowNet3D: Learning scene flow in 3D point clouds. In *CVPR*, pages 529–537, 2019. 3
- [24] Yuan Liu, Sida Peng, Lingjie Liu, Qianqian Wang, Peng Wang, Theobalt Christian, Xiaowei Zhou, and Wenping Wang. Neural rays for occlusion-aware image-based rendering. In *CVPR*, 2022. 2
- [25] Ricardo Martin-Brualla, Noha Radwan, Mehdi S. M. Sajjadi, Jonathan T. Barron, Alexey Dosovitskiy, and Daniel Duckworth. NeRF in the Wild: Neural radiance fields for unconstrained photo collections. In *CVPR*, 2021. 2
- [26] Ben Mildenhall, Peter Hedman, Ricardo Martin-Brualla, Pratul P. Srinivasan, and Jonathan T. Barron. NeRF in the dark: High dynamic range view synthesis from noisy raw images. In *CVPR*, pages 16169–16178, 2022. 2
- [27] Ben Mildenhall, Pratul P. Srinivasan, Matthew Tancik, Jonathan T. Barron, Ravi Ramamoorthi, and Ren Ng. NeRF: Representing scenes as neural radiance fields for view synthesis. In *ECCV*, 2020. 2, 6, 7

- [28] Michael Niemeyer and Andreas Geiger. GIRAFFE: Representing scenes as compositional generative neural feature fields. In *CVPR*, pages 11453–11464, June 2021. 2
- [29] Michael Niemeyer, Lars Mescheder, Michael Oechsle, and Andreas Geiger. Occupancy Flow: 4D reconstruction by learning particle dynamics. In *ICCV*, 2019. 3
- [30] Julian Ost, Fahim Mannan, Nils Thuerey, Julian Knodt, and Felix Heide. Neural scene graphs for dynamic scenes. In *CVPR*, pages 2856–2865, June 2021. 2
- [31] Albert Pumarola, Enric Corona, Gerard Pons-Moll, and Francesc Moreno-Noguer. D-NeRF: Neural Radiance Fields for Dynamic Scenes. In *CVPR*, 2020. 2
- [32] Johannes Lutz Schönberger and Jan-Michael Frahm. Structure-from-Motion Revisited. In *CVPR*, 2016. 7
- [33] Johannes Lutz Schönberger, Enliang Zheng, Marc Pollefeys, and Jan-Michael Frahm. Pixelwise View Selection for Unstructured Multi-View Stereo. In *ECCV*, 2016. 7
- [34] Katja Schwarz, Yiyi Liao, Michael Niemeyer, and Andreas Geiger. GRAF: Generative radiance fields for 3D-aware image synthesis. In *NeurIPS*, 2020. 2
- [35] Pratul P. Srinivasan, Boyang Deng, Xiuming Zhang, Matthew Tancik, Ben Mildenhall, and Jonathan T. Barron. NeRV: Neural reflectance and visibility fields for relighting and view synthesis. In *CVPR*, 2021. 2
- [36] Zachary Teed and Jia Deng. RAFT: Recurrent All-Pairs field transforms for optical flow. In Andrea Vedaldi, Horst Bischof, Thomas Brox, and Jan-Michael Frahm, editors, *ECCV*, pages 402–419, Cham, 2020. 4, 7
- [37] Edgar Tretschk, Ayush Tewari, Vladislav Golyanik, Michael Zollhöfer, Christoph Lassner, and Christian Theobalt. Non-rigid neural radiance fields: Reconstruction and novel view synthesis of a dynamic scene from monocular video. In *ICCV*, pages 12939–12950, 2021. 2, 3, 6, 8
- [38] Emanuele Trucco and Konstantinos Plakas. Video tracking: a concise survey. *IEEE Journal of oceanic engineering*, 31(2):520–529, 2006. 3
- [39] Yi-Hsuan Tsai, Ming-Hsuan Yang, and Michael J Black. Video segmentation via object flow. In *CVPR*, pages 3899–3908, 2016. 3
- [40] S. Vedula, S. Baker, P. Rander, R. Collins, and T. Kanade. Three-dimensional scene flow. In *ICCV*, volume 2, pages 722–729 vol.2, 1999. 2, 3
- [41] Longguang Wang, Yulan Guo, Li Liu, Zaiping Lin, Xinpu Deng, and Wei An. Deep video super-resolution using HR optical flow estimation. *IEEE TIP*, 29:4323–4336, 2020. 3
- [42] Peng Wang, Lingjie Liu, Yuan Liu, Christian Theobalt, Taku Komura, and Wenping Wang. NeuS: Learning neural implicit surfaces by volume rendering for multi-view reconstruction. *NeurIPS*, 2021. 2
- [43] Zhou Wang, A.C. Bovik, H.R. Sheikh, and E.P. Simoncelli. Image quality assessment: from error visibility to structural similarity. *IEEE TIP*, 13(4):600–612, 2004. 8
- [44] Chung-Yi Weng, Brian Curless, Pratul P. Srinivasan, Jonathan T. Barron, and Ira Kemelmacher-Shlizerman. HumanNeRF: Free-viewpoint rendering of moving people from monocular video. In *CVPR*, pages 16210–16220, June 2022. 2, 3
- [45] Tianhao Wu, Fangcheng Zhong, Andrea Tagliasacchi, Forrester Cole, and Cengiz Öztireli. D2NeRF: Self-supervised decoupling of dynamic and static objects from a monocular video. *NeurIPS*, abs/2205.15838, 2022. 2, 3
- [46] Wenqi Xian, Jia-Bin Huang, Johannes Kopf, and Changil Kim. Space-time neural irradiance fields for free-viewpoint video. In *CVPR*, pages 9421–9431, 2021. 2, 3
- [47] Yuanbo Xiangli, Linning Xu, Xingang Pan, Nanxuan Zhao, Anyi Rao, Christian Theobalt, Bo Dai, and Dahua Lin. BungeeNeRF: Progressive neural radiance field for extreme multi-scale scene rendering. In *ECCV*, 2022. 2
- [48] Qiangeng Xu, Zexiang Xu, Julien Philip, Sai Bi, Zhixin Shu, Kalyan Sunkavalli, and Ulrich Neumann. Point-NeRF: Point-based neural radiance fields. *CVPR*, 2022. 2
- [49] Jae Shin Yoon, Kihwan Kim, Orazio Gallo, Hyun Soo Park, and Jan Kautz. Novel view synthesis of dynamic scenes with globally coherent depths from a monocular camera. In *CVPR*, June 2020. 6
- [50] Alex Yu, Vickie Ye, Matthew Tancik, and Angjoo Kanazawa. pixelNeRF: Neural radiance fields from one or few images. In *CVPR*, 2021. 2, 7
- [51] Richard Zhang, Phillip Isola, Alexei A. Efros, Eli Shechtman, and Oliver Wang. The unreasonable effectiveness of deep features as a perceptual metric. In *CVPR*, June 2018. 7, 8